



HAL
open science

Anisotropic adaptive mesh procedure for computing very thin hyperbolic shells

C. de Souza, F B Échet, Dominique Leguillon, É Sanchez-Palencia

► **To cite this version:**

C. de Souza, F B Échet, Dominique Leguillon, É Sanchez-Palencia. Anisotropic adaptive mesh procedure for computing very thin hyperbolic shells. BIT Numerical Mathematics, 2008, 48 (2), pp.357-387. 10.1007/s10543-008-0183-y . hal-00343916

HAL Id: hal-00343916

<https://hal.science/hal-00343916>

Submitted on 20 Mar 2024

HAL is a multi-disciplinary open access archive for the deposit and dissemination of scientific research documents, whether they are published or not. The documents may come from teaching and research institutions in France or abroad, or from public or private research centers.

L'archive ouverte pluridisciplinaire **HAL**, est destinée au dépôt et à la diffusion de documents scientifiques de niveau recherche, publiés ou non, émanant des établissements d'enseignement et de recherche français ou étrangers, des laboratoires publics ou privés.

ANISOTROPIC ADAPTIVE MESH PROCEDURE FOR COMPUTING VERY THIN HYPERBOLIC SHELLS

C. DE SOUZA¹, F. BÉCHET², D. LEGUILLON³, É. SANCHEZ-PALENCIA³

¹*Travessa Arnaldo Lopes Silva, 171 - Bloco A - Ap. 903 - STIEP - Salvador - Bahia -
Brésil 41770-055.*

email: carlosaugustodesouza@gmail.com

²*Laboratoire de Mécanique de Lille, Boulevard Paul Langevin, 59655 Villeneuve d'Ascq
Cédex, France.*

email: fabien.bechet@gmail.com

³*Institut Jean Le Rond d'Alembert, Université Paris VI, 4 place Jussieu, Paris, France.*

email: {leguillo@lmm.jussieu.fr,sanchez@lmm.jussieu.fr}

Abstract.

This paper is devoted to the study of the mechanical behavior of thin elastic shells when their relative thickness ε tends to zero. We focus on the case of hyperbolic shells whose middle surface has principal curvatures of opposite signs everywhere. We use the Koiter model to describe the mechanical behavior of the shell. The corresponding system, which depends on the relative thickness ε , is elliptic except at the limit for $\varepsilon = 0$ where it is hyperbolic. In a first part, we study theoretically the phenomena of internal layers appearing during the singular perturbation process, when the loading is somewhat singular. These layers have very different structures either they are along or across the asymptotic lines of the middle surface of the shell. Moreover, we may have pseudo-reflections when a part of the boundary is not along an asymptotic line of the surface. In any case, the layers become very thin when ε tends to zero and the displacements inside the layers tends to infinity. In order to have a good description of the singularities of the displacements inside the layers, we propose here to use an anisotropic and adaptive mesh procedure. In a second part, we will present numerical computations performed with such meshes. They enable us to approach accurately the singularities inside the layers predicted by the theory. Finally, we test the behavior of the remeshing procedure when the shell is non-inhibited.

AMS subject classification (2000): 74B05, 74K25, 74S05, 76M45, 35A21, 65N50

Key words: Shell theory, Singular perturbation, Anisotropic mesh, Internal layers.

1 Introduction

In this paper, we consider thin elastic shells of relative thickness ε and their asymptotic behavior when ε tends to zero. Classically, asymptotic studies of such structures when $\varepsilon \searrow 0$ give either a membrane model or a pure bending one. To have both contributions (membrane and bending), we use the Koiter model [16] although it is not an asymptotic model. The variational form of the

Koiter model can be written [4, 19]:

$$(1.1) \quad \begin{aligned} &\text{Find } u \in V, \text{ such as, } \forall v \in V : \\ &a_m(u^\varepsilon, v) + \varepsilon^2 a_b(u^\varepsilon, v) = b(v) \end{aligned}$$

It contains two parts: a_m represents the membrane effects and $\varepsilon^2 a_b$ the bending effects proportional to ε^2 . For $\varepsilon > 0$, the corresponding system is always elliptic and classical results of regularity hold true. The solution belongs to the energy space of the variational problem denoted V , which is essentially $H^1 \times H^1 \times H^2$ (for the tangent and normal components of the displacement vector, respectively) with the kinematic boundary conditions. The limit problem (when $\varepsilon = 0$) of the Koiter shell model is very different either the space

$$(1.2) \quad G = \{v \in V; a_m(v, v) = 0\} = \{v \in V; \gamma_{\alpha\beta}(v) = 0\}$$

reduces to $\{0\}$ or not, $\gamma_{\alpha\beta}$ denoting the covariant components of the membrane strain tensor which writes:

$$(1.3) \quad \gamma_{\alpha\beta}(u) = \frac{1}{2}(D_\alpha u_\beta + D_\beta u_\alpha) - b_{\alpha\beta} u_3$$

where $D_\alpha u_\beta = \partial_\alpha u_\beta - \Gamma_{\alpha\beta}^\lambda u_\lambda$ denotes the covariant derivative of u_β with respect to α , and $b_{\alpha\beta}$ are the covariant components of the second fundamental form accounting for curvatures.

When $G = \{0\}$, the shell is called *inhibited* or *geometrically rigid*: the middle surface does not admit inextensional displacements, *i. e.* displacement leaving the metrics unchanged (in the linearized sense). Oppositely, when $G \neq \{0\}$, the shell is not inhibited. The nature of G depends only on the geometry of the middle surface and on boundary conditions [19].

In the case of inhibited shells, the asymptotic process when $\varepsilon \searrow 0$ is a singular perturbation problem since the bending part contains the highest order derivatives. As the normal displacement u_3 is in H^2 when $\varepsilon > 0$ but only in L^2 (at best) when $\varepsilon = 0$, boundary layers appear during the asymptotic process. The limit problem is the membrane problem which writes:

$$(1.4) \quad a_m(u^0, v) = b(v)$$

Moreover, the limit problem is hyperbolic (respectively parabolic or elliptic) if the middle surface of the shell is respectively hyperbolic (respectively parabolic or elliptic). When the middle surface is parabolic or hyperbolic, the limit problem has real characteristic lines (corresponding to the asymptotic lines of the surface) (see for instance [19]). Consequently, a non-smooth loading causes singularities at the limit that may propagate along these lines. In this case, when $\varepsilon \searrow 0$, internal layers appear. It should be noted that, in most examples, the singularities are so important that a good description of the layers amounts to a good description of the whole solution.

The very peculiar structure of the limit problem implies that "very singular" solutions may be provoked by "moderate" singularities of the data. For instance, in certain cases, singularities of the solutions are "two steps" more singular than the data (it means that, as an example, a jump of the second derivatives of the normal force imply a jump of the normal displacement itself, and so on). Consequently, the corresponding theory is currently handled in the framework of *distribution theory* (including δ -like and even more singular elements, which appear in applications). Appendix A contains a few indications in this context.

Obviously, a very large variety of situations may appear according to the geometry of the middle surface. In this paper, we focus on hyperbolic shells *i. e.* the principal curvatures of the middle surface of the shell have (everywhere) opposite signs (this occurs when $b_{11}b_{22} - b_{12}^2 < 0$). For this kind of shells, *reflection phenomena* may also appear [13, 15]. When an internal layer reaches a non-characteristic boundary, singularities may reflect and propagate along the two characteristics starting from the intersection of the internal layer and the boundary. As these reflections do not satisfy laws of classical reflection, they are often called "pseudo reflections" (in most cases, the reflected singularity is "one step" less singular than the incident one; several cases were described in [15]).

Along boundary and internal layers, singularities may be very sharp (as the Dirac mass on the curve, and even more singular), containing most of the deformation energy. Obviously, for small ε , the singularities of the limit problem are replaced by layers, so that a local refinement of the mesh nearby them is highly pertinent. Moreover, because of the phenomenon of propagation of singularities along the characteristics, the local structure of the layers is somewhat anisotropic. So, anisotropic meshes with higher refinement across the layer than along it are most fitted for computing such kind of problems. But the simultaneous presence of several kinds of such singularities in a problem makes it difficult to foresee a good mesh before solving (even approximately) the problem. In addition, the construction of such meshes is made practically impossible by the presence of phenomena of reflection of the singularities at the boundaries. These peculiarities are analogous to those of computation in fluid mechanics problems. Precisely, the main aim of this paper is to show the reliability and efficiency in shell problems of the two-dimensional anisotropic mesh generator BAMG developed by INRIA¹ for fluid flow problems. More precisely, this adaptive and anisotropic mesh procedure, based on iterative automatic mesh generation, was applied previously [2, 3, 10, 11] to singularities in various situations of inhibited shells. In the present paper, we apply it to hyperbolic shells in the various situations analogous to those of the "real word", with simultaneous presence of several kinds of singularities, including reflections (in section 4) and both non-inhibited regions and singularities in inhibited regions (in section 5).

In the case of non-inhibited shells (*i. e.* the middle surface is not geometrically rigid), the difficulties are of a different nature. In order to minimize

1. Institut National de Recherche en Informatique et Automatique

elastic energy, the natural trend of the solution (for small ε) is to perform "pure bendings", which avoid the (large) membrane energy, and only use the (small) bending energy. This implies very particular deformations where the asymptotic lines of the surface play a peculiar role, inducing anisotropic deformation. Let us explain this a little. The elements of G are solutions of the "rigidity system":

$$(1.5) \quad \begin{cases} \gamma_{11} = D_1 u_1 - b_{11} u_3 = 0 \\ \gamma_{22} = D_2 u_2 - b_{22} u_3 = 0 \\ \gamma_{12} = \frac{1}{2}(D_1 u_2 + D_2 u_1) - b_{12} u_3 = 0 \end{cases}$$

which (after eliminating one of the unknowns, u_3 for instance, from the third equation) is a hyperbolic system of first order with two equations and two unknowns. The characteristics of the system are the asymptotic curves of the middle surface, which play in some sense the role of "local infinitesimal hinges" allowing infinitesimal rotations along them. This is particularly evident in the case when the surface is ruled, made of family of straight lines (called "generators"): the surface admits (the boundary conditions are not taken into account) displacements consisting of arbitrary infinitesimal rotations around the generators, which preserve the intrinsic metrics of the surface. Clearly, such kind of displacements is highly anisotropic along the generators. The simplest and clearest example is that of the "ruled quadrics" (the hyperbolic hyperboloid and the hyperbolic paraboloid) which have two families of such generators. All the isometric deformations are made of the above mentioned rotations around the two families of generators. According to boundary conditions, one or both rotations may be (partially or totally) impeached, giving various specific examples of subspace G (the case when the boundary conditions impeach both rotations everywhere is the "inhibited" case). We shall see in section 5 examples of such situations. The general case (when the characteristics are not straight) is essentially analogous "at the leading order" of deformation, whereas other smoother terms are also present.

The reasons of the difficulties of computation of solutions in the subspace G of pure bendings are classical, as the ε -dependent problem takes the form of a penalty problem, which classically induces *locking* (see for instance [1, 17]). Incidentally, it should be mentioned that the difficulties of computation of singularities in the inhibited case may be interpreted in terms of locking (in fact a local locking inside the layers) via a re-scaling of the variables and unknowns. Indeed, after such re-scaling, the problem describing the singularities exhibits a G -like subspace describing the limit behaviour (see [8, 18]).

Obviously, the reliability of the above mentioned automatic procedure of adaptive anisotropic meshes should also be accurate for other shapes of the shell (elliptic and parabolic shells), but this question will not be discussed here, as it implies very different singular behaviors. For instance, the reader can refer to [2, 3] for the case of elliptic shells.

The paper is organized as follows. In section 2, we study the membrane limit problem for a hyperbolic shell subjected to a singular loading. We exhibit the singularities of the three displacements for three different loadings. Section 3 is devoted to numerical computation of the Koiter shell model for very small thicknesses using the anisotropic and adaptive mesh procedure for the three loadings considered before. These examples prove the efficiency of such a technique to obtain accurate results inside the layers. In particular, the advantage of an adaptive mesh with respect to an uniform one is shown. In section 4, we show how useful this numerical procedure is when pseudo-reflection of singularities occur on boundaries. Finally, the last section is devoted to numerical computation for non-inhibited problems where we study how behaves the remeshing procedure in more complex situations where membrane and bending effects dominate in different areas of the shells.

2 The limit problem for a hyperbolic inhibited shell

Let us consider a shell whose middle surface is hyperbolic and boundary conditions such as the shell is inhibited². As we mentioned in the introduction, in that case, the limit problem when ε tends to zero is the membrane problem. The limit solution u^0 satisfies the *membrane system*:

$$(2.1) \quad \begin{cases} -D_\beta T^{\alpha\beta} = f^\beta \\ -b_{\alpha\beta} T^{\alpha\beta} = f^3 \end{cases}$$

with the associated boundary conditions and where

$$(2.2) \quad T^{\alpha\beta} = A^{\alpha\beta\lambda\mu} \gamma_{\lambda\mu}$$

denote the components of the membrane stress tensor and $\gamma_{\alpha\beta}$ are the components of the strain tensor given in term of the unknowns u_i by the expressions (1.5). The coefficients $A^{\alpha\beta\lambda\mu}$ are the isotropic linear elastic constitutive law coefficients defined by (see [4]):

$$(2.3) \quad A^{\alpha\beta\lambda\mu} = \frac{E}{2(1+\nu)} \left[a^{\alpha\lambda} a^{\beta\mu} + a^{\alpha\mu} a^{\beta\lambda} + \frac{2\nu}{1-\nu} a^{\alpha\beta} a^{\lambda\mu} \right]$$

where ν and E are respectively the Poisson ratio and the Young modulus.

Replacing in (2.1) the expressions (2.2) of $T^{\alpha\beta}$, we obtain a system of partial differential equations characterizing the displacement u (see [2] for more details). Another way to solve the membrane problem is to compute first the tensions $T^{\alpha\beta}$ from (2.1). Then, thanks to equation (2.2), we can find the components of the membrane strain $\gamma_{\lambda\mu}$ and finally the displacements u . Note that in this second case, it is easier to use the inverse relation:

$$(2.4) \quad \gamma_{\lambda\mu} = B_{\alpha\beta\lambda\mu} T^{\alpha\beta}$$

2. For that, every asymptotic line has to be clamped or simply supported at least at one point.

where $B_{\alpha\beta\lambda\mu}$ are the membrane compliance coefficients.

Taking a special parametrization (y^1, y^2) , where the coordinate lines are the asymptotic curves of the middle surface, the covariant components $b_{\alpha\beta}$ of the second fundamental form reduce to $b_{11} = b_{22} = 0$ and $b_{12} \neq 0$. In what follows, we will consider the case of a normal loading, giving the most singular results for displacements. We then have:

$$(2.5) \quad f^1 = f^2 = 0$$

It enables us to write the membrane system (2.1) like follows:

$$(2.6) \quad \begin{cases} D_1 T^{11} + D_2 T^{12} = 0 \\ D_2 T^{22} + D_1 T^{12} = 0 \\ -2b_{12} T^{12} = f^3 \end{cases}$$

In the sequel, this system will be used to determine the higher order term singularity of the three displacements (solutions of the limit problem) for various loadings. Numerical simulations using F. E. method and an adaptive mesh procedure will confirm this result when $\varepsilon \searrow 0$.

2.1 Example of a hyperbolic paraboloid

In what follows, we will consider the case of a shell whose middle surface S is a hyperbolic paraboloid (see Fig. 2.1). The surface S is defined by the mapping (Ω, Ψ) with:

$$(2.7) \quad \Omega = \{(y^1, y^2) \in \mathbb{R}^2, (y^1, y^2) \in [-L, L]^2\}$$

and

$$(2.8) \quad \Psi(y^1, y^2) = \left(y^1, y^2, \frac{y^1 y^2}{c} \right)$$

We will consider the values $L = 50 \text{ mm}$ and $c = 250 \text{ mm}$ for the numerical computations. Moreover, the material considered is isotropic and homogeneous, with a Young modulus $E = 28500 \text{ MPa}$ and a Poisson ratio $\nu = 0.4$. The relative thickness ε is taken as the ratio "thickness/2L" which gives in our case $\varepsilon = 0.01 \times \text{thickness}$.

This specific parametrization corresponds to that of the asymptotic lines. Indeed, the mapping (Ω, Ψ) implies the following covariant coefficients of the first (2.9) and second (2.10) fundamental forms:

$$(2.9) \quad a_{\alpha\beta} = \begin{pmatrix} 1 + \frac{(y^2)^2}{c^2} & \frac{y^1 y^2}{c^2} \\ \frac{y^1 y^2}{c^2} & 1 + \frac{(y^1)^2}{c^2} \end{pmatrix}$$

$$(2.10) \quad b_{11} = b_{22} = 0 \quad b_{12} = b_{21} = \frac{1}{\sqrt{c^2 + (y^1)^2 + (y^2)^2}}$$

The only non-vanishing Christoffel symbol used in this paper is

$$(2.11) \quad \Gamma_{12}^1 = \frac{y^2}{c^2 + (y^1)^2 + (y^2)^2}$$

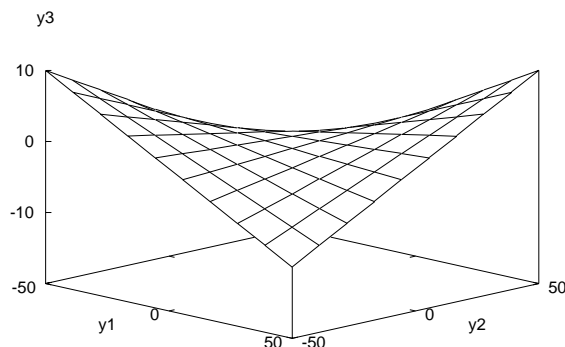


Figure 2.1: The hyperbolic paraboloid

The middle surface is then uniformly hyperbolic. The asymptotic directions satisfy

$$(2.12) \quad 2b_{12}(dy^1)(dy^2) = 0$$

which gives, as $b_{12} > 0$, two distinct families of asymptotic curves:

$$(2.13) \quad y^1 = \text{const} \quad \text{and} \quad y^2 = \text{const}$$

The asymptotic curves play an important role as they correspond to the characteristic lines of the membrane and rigidity systems [19]. We will see that if the loading is somewhat singular along an asymptotic line, the resulting displacements will be singular on the whole asymptotic line. In what follows, we shall call these lines indifferently "asymptotic" or "characteristic". We are now considering the case when a normal loading f^3 is singular along a characteristic line, and we shall exhibit the leading order singularities and their propagative character. The case of singularity along non-characteristic lines is similar to that of elliptic or parabolic shells which were considered in [2, 3]. The terminology used for singularities is detailed in appendix A.

2.2 Singularities of the displacements due to a loading singular on the line $y^1 = 0$

Let f^3 be singular on a characteristic line $y^1 = 0$. We shall write it under the form:

$$(2.14) \quad f^3 = \psi(y^1) \varphi(y^2)$$

where $\psi(y^1)$ plays the role of S_0 (see (A.1) in appendix A for more details) and $\varphi(y^2)$ denotes its weight along $y^1 = 0$.

Let us study the system (2.6) near $y^1 = 0$. It becomes:

$$(2.15) \quad \begin{cases} D_1 T^{11} + D_2 T^{12} = 0 \\ D_2 T^{22} + D_1 T^{12} = 0 \\ -2b_{12}(0, y^2) T^{12} = f^3 \end{cases}$$

From the third equation of (2.15), we get:

$$(2.16) \quad T^{12} = \tau^{12}(y^2) \psi(y^1)$$

with

$$(2.17) \quad \tau^{12}(y^2) = -\frac{1}{2b_{12}(0, y^2)} \varphi(y^2)$$

Replacing T^{12} in the second equation of (2.15), we obtain:

$$(2.18) \quad \partial_2 T^{22} + \Gamma_{12}^1(0, y^2) T^{22} = -\tau^{12}(y^2) \psi'(y^1) + \dots$$

where $\Gamma_{\alpha\beta}^\gamma$ are the Christoffel symbols and \dots denotes lower order terms. We then deduce the leading term of T^{22} :

$$(2.19) \quad T^{22} = \tau^{22}(y^2) \psi'(y^1) + \dots$$

with

$$(2.20) \quad \partial_2 \tau^{22}(y^2) + \Gamma_{12}^1 \tau^{22}(y^2) = -\tau^{12}(y^2)$$

and where \dots denotes lower order terms.

Finally, replacing T^{12} in the first equation of (2.15), we obtain the expression of T^{11} :

$$(2.21) \quad T^{11} = \tau^{11}(y^2) \psi^{(-1)}(y^1) + \dots$$

with

$$(2.22) \quad \tau^{11}(y^2) = -\partial_2 \tau^{12}(y^2)$$

where $\psi^{(-1)}$ is such that $\partial_1 \psi^{(-1)}(y^1) = \psi(y^1)$ (see appendix A).

The most singular tension is T^{22} which is one order more singular than $\psi(y^1)$. Using the inverse constitutive law (2.4), we get the system:

$$(2.23) \quad \begin{cases} D_1 u_1^0 = B_{1122} \tau^{22}(y^2) \psi'(y^1) + \dots \\ D_2 u_2^0 = B_{2222} \tau^{22}(y^2) \psi'(y^1) + \dots \\ \frac{1}{2}(D_1 u_2^0 + D_2 u_1^0) - 2b_{12} u_3^0 = 2B_{1222} \tau^{22}(y^2) \psi'(y^1) + \dots \end{cases}$$

We deduce u_1^0 and u_2^0 respectively from the first and the second equations of (2.23). Finally, we get u_3^0 from the third equation of (2.23) where $\partial_1 u_2^0$ is more singular than the right hand side. We obtain the general form of the displacements (only the most singular terms with respect to y^1) in the vicinity of the line $y^1 = 0$:

$$(2.24) \quad \begin{cases} u_1^0(y^1, y^2) = U_1(y^2) \psi(y^1) + \dots \\ u_2^0(y^1, y^2) = U_2(y^2) \psi'(y^1) + \dots \\ u_3^0(y^1, y^2) = U_3(y^2) \psi''(y^1) + \dots \end{cases} \quad \text{with} \quad \begin{cases} U_1(y^2) = B_{1122} \tau^{22}(y^2) \\ \partial_2 U_2(y^2) = B_{2222} \tau^{22}(y^2) \\ U_3(y^2) = \frac{1}{4b_{12}} U_2(y^2) \end{cases}$$

We then observe that the leading order terms of the singularities are defined up to two arbitrary constants (from the two first order equations: (2.20) and the second one of the right of (2.24)). They are easily defined using the boundary conditions at the first order. Two aspects of the results must be underlined. On one hand, u_1^0 , u_2^0 and u_3^0 are respectively 0, 1 and 2 order(s) more singular than f^3 (their highest order singularity are respectively ψ , ψ' and ψ''). On the other hand, the singularities propagate along the corresponding generator $y^1 = 0$. Indeed, U_1 , U_2 and U_3 do not vanish when $\varphi(y^2)$ vanishes. As they are primitives of $\varphi(y^2)$ with respect to y^2 , they contain smooth terms generally different from 0. This implies that the singular terms in y^1 exist all along the characteristic line $y^1 = 0$ even if $\varphi(y^2)$ (and consequently f^3) vanishes.

2.3 The three cases of loading

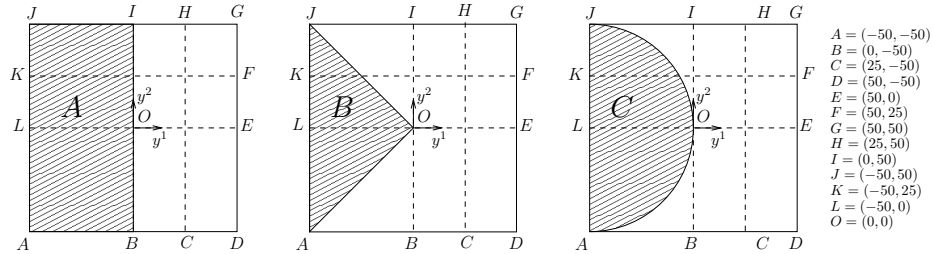


Figure 2.2: The three loadings considered on the domain Ω : (A) discontinuity on a characteristic line ($[BI]$), (B) discontinuity on non-characteristic lines ($[AO]$ and $[JO]$), (C) discontinuity on a non-characteristic curve ($[AOJ]$), but tangent to a characteristic line ($[BI]$)

The three cases of loading are presented on Fig. 2.2. An uniform normal pressure, proportional to the thickness is applied respectively in the regions A,

B , and C . Let us exhibit the singularities of these three loadings near the line $y^1 = 0$ in the previous context.

• **Loading A**

The expression of the loading A is³ $f^3 = H(-y^1)$. The singularity near $y^1 = 0$ is then:

$$(2.25) \quad \psi(y^1) = H(-y^1) \quad \text{and} \quad \varphi(y^2) = 1$$

• **Loading B**

The expression of the singularity of loading B near $y^1 = 0$ is not direct. For a fixed $y^1 < 0$, we have:

$$(2.26) \quad f^3 = H(y^2 - y^1) - H(y^2 + y^1) = (-2y^1) \frac{H(y^2 - y^1) - H(y^2 + y^1)}{-2y^1}$$

and f^3 vanishes for $y^1 > 0$. It then appears that the expression of the singularity of the loading B near $y^1 = 0$ is finally:

$$(2.27) \quad f^3 \approx -2y^1 H(-y^1) \delta(y^2)$$

where δ denotes the Dirac mass (see appendix A). A rigorous proof of (2.27) may be obtained using distributions acting on test functions. This gives:

$$(2.28) \quad \psi(y^1) = y^1 H(-y^1) \quad \text{and} \quad \varphi(y^2) = -2\delta(y^2)$$

A similar singularity (*i. e.* with the same order) exist along $y^2 = 0$.

• **Loading C**

The expression of the singularity of the loading C near by the line $y^1 = 0$ is obtained in the same way. For a fixed $y^1 < 0$, we have:

$$(2.29) \quad f^3 = H(y^2 + s) - H(y^2 - s)$$

where s has to be expressed using the equation of the circle. This finally gives:

$$(2.30) \quad f^3 \approx 2\sqrt{2L}\sqrt{-y^1} H(-y^1) \delta(y^2)$$

so that we have:

$$(2.31) \quad \psi(y^1) = \sqrt{-y^1} H(-y^1) \quad \text{and} \quad \varphi(y^2) = 2\sqrt{2L}\delta(y^2)$$

Obviously, the singularity of $\psi(y^1)$ in (2.31) is not very classical and it is not an element of the classical chain (A.2) (see appendix A). But it may be taken as S_0 for a chain of the type (A.1) describing the singularities of the solutions.

3. $H(\cdot)$ denotes the classical Heaviside jump function.

2.4 The singularities of the resulting displacements

Using (2.24), we deduce the singularities of the three displacements at $y^1 = 0$ for each loading. The corresponding results are summarized in Table 2.1.

Loading A	Loading B
$u_1^0 = U_1(y^2)H(-y^1)$	$u_1^0 = U_1(y^2)y^1H(-y^1)$
$u_2^0 = U_2(y^2)\delta(-y^1)$	$u_2^0 = U_2(y^2)H(-y^1)$
$u_3^0 = U_3(y^2)\delta'(-y^1)$	$u_3^0 = U_3(y^2)\delta(-y^1)$
Loading C	
$u_1^0 = U_1(y^2)\sqrt{-y^1} H(-y^1)$	
$u_2^0 = U_2(y^2)(-y^1)^{-\frac{1}{2}}H(-y^1)$	
$u_3^0 = U_3(y^2)\frac{d}{dy^1}\left((-y^1)^{-\frac{1}{2}}H(-y^1)\right)$	

Table 2.1: Orders of the singularities of the three displacements for the three loadings

where $\frac{d}{dy^1}$ is the derivative in the sense of distributions.

3 Numerical computations using adaptive meshes

3.1 Numerical procedure

The numerical computations have been performed with the finite element software MODULEF using the DKTC element [4]. The mesh is realized on the 2D domain of the local mapping of the middle surface, which avoids geometrical approximations of planar facet decomposition. According to the general considerations in the introduction, we need anisotropic adaptive meshes more refined across the layers than along them. To create such meshes, we use the "bidimensional anisotropic mesh generator" BAMG, developed by INRIA. Error estimates for finite elements using anisotropic meshes inside of layers in the case of parabolic shells have been presented in [20, 21]. It leads to a better description of the singularities with a reduced number of elements.

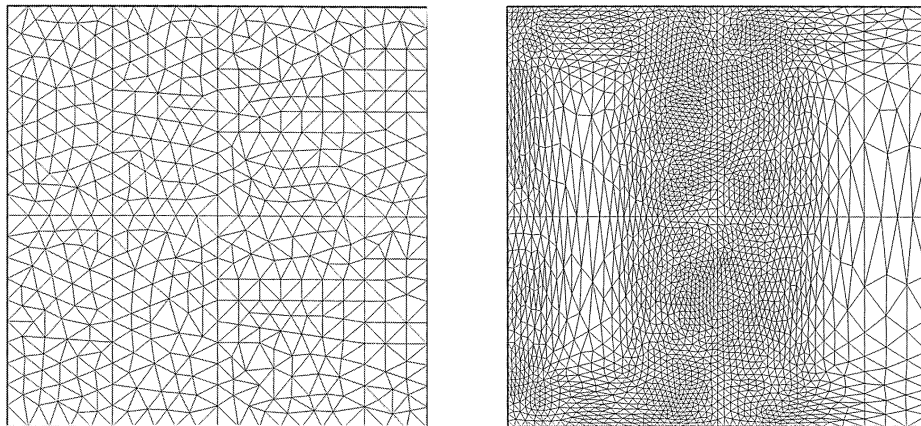
The software BAMG performs an anisotropic mesh adaptation using *metric control* technique. It was initially developed to compute supersonic aerodynamic flows which exhibit shock waves [5, 6, 7]. It has already been used with success for shell and shell-like problems computations in [2, 3, 10, 11]. A new mesh is

generated with a modified metrics. To do this, BAMG uses the Hessian of the solution at each step of an iteration to define a new Riemannian metrics for the next step: lengths are increased (respectively diminished) in the areas and the directions where the second order derivatives are large (respectively small) (see [12]). Consequently, the mesh is refined (respectively coarsened) when the second order derivatives are large (respectively small). For more details, one may refer to [2, 3, 10]. For the shell problems considered here, we use the bending displacement u_3^e for the remeshing procedure. Then the mesh will be refined in the areas where the second order derivatives of u_3^e are large. They correspond to the areas where the bending is important.

It should be emphasized that the very point of the procedure relies on the construction of a new (non Euclidean, but Riemannian) metrics whose length element is defined with the Hessian of the solution (at the previous step of the iterative procedure). In terms of this metrics, which remains hidden, the mesh is (more or less) uniform and isotropic. The triangles are only elongated in terms of the usual Euclidean metrics, whereas they are equilateral in the hidden metrics, which is essentially used in the computation. It is known that elongated triangles with angles nearby π may give trouble; but such difficulty was never encountered with BAMG, as the "effective shape" of the triangles in the "effective" (but hidden) metrics is (almost) equilateral.

3.2 Numerical results for loading A

First, let us observe the adaptation process at some iterations.



(a) Initial mesh

(b) Iteration 2

Figure 3.1: Evolution of the mesh during the adaptation process (iterations 0 and 2)

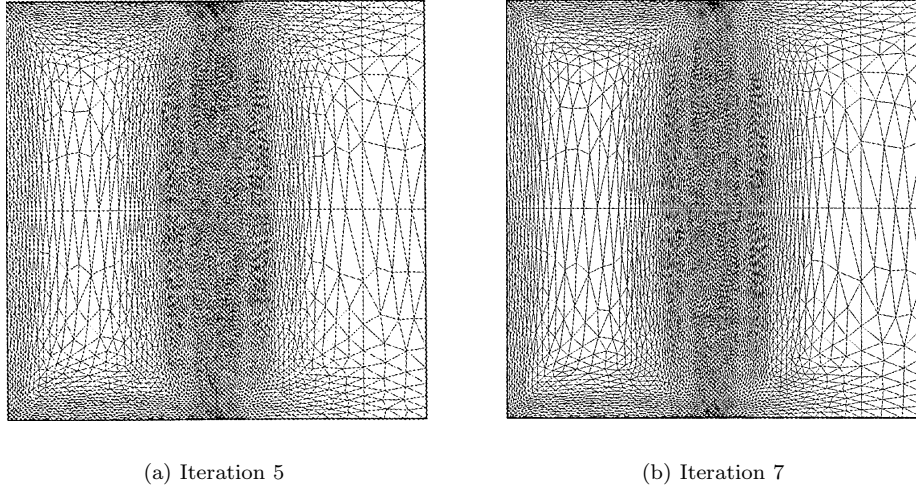


Figure 3.2: Evolution of the mesh during the adaptation process (iterations 5 and 7)

The initial mesh is quite uniform (Fig. 3.1(a)). At the first iteration, anisotropy is not very apparent (the initial mesh was too coarse). From the second iteration, the elements start to become clearly anisotropic and we can observe the layers which appear progressively. The final mesh (Fig. 3.2(b)) is highly anisotropic and non-uniform: the elements are small and lengthened in the layers, especially along $y^1 = 0$ corresponding to an internal layer. The displacements at various iterations and for two relative thicknesses are plotted on Figs. 3.3(a) and 3.3(b).

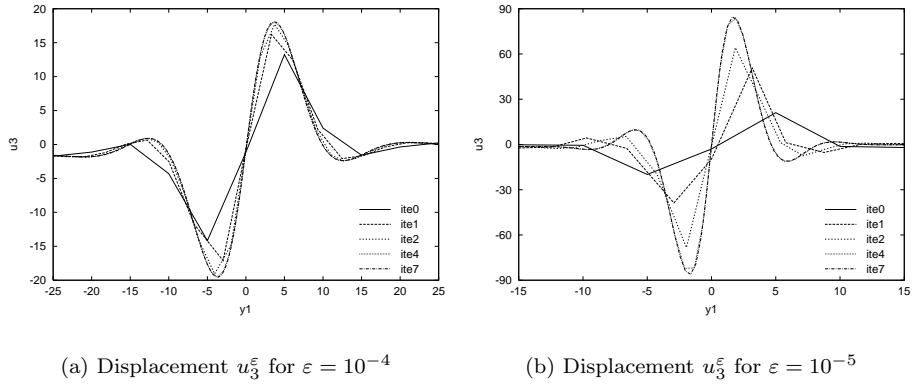


Figure 3.3: Displacement u_3 at $y^2 = 0$ for $y^1 \in [-25, 25]$ and at various iterations for loading A

In Fig. 3.3(a), we can see that the results are nearly the same at the 4th and the 7th iteration for $\varepsilon = 10^{-4}$ as the process has nearly converged. The results obtained with the initial mesh and at the first and second iterations are quite far from those of the 7th. Subsequent iterations do not improve the solution.

The efficiency of the adaptive process is more visible for $\varepsilon = 10^{-5}$ (Fig. 3.3(b)). For this thickness, the process takes longer to converge, and a refinement is very useful to get accurate results. The displacements at the 7th iteration are about twice larger than those at the first iteration. This shows the pertinence of such an automatic anisotropic procedure of refinement.

3.2.1 Convergence toward the limit problem

The solutions (in fact sections of them at $y^2 = 25$) of the three displacements for various values of the relative thickness ε are represented on figures 3.4 to 3.6.

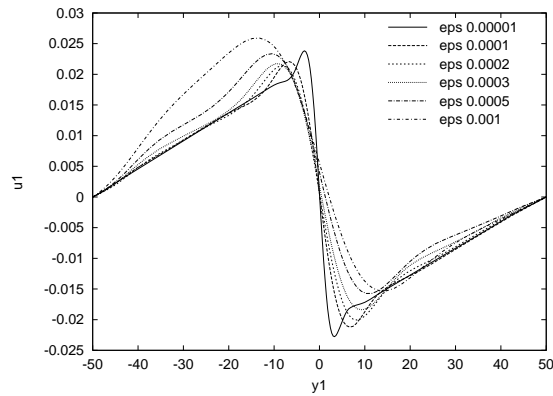


Figure 3.4: Displacement u_1^ε at $y^2 = 25$ for various ε

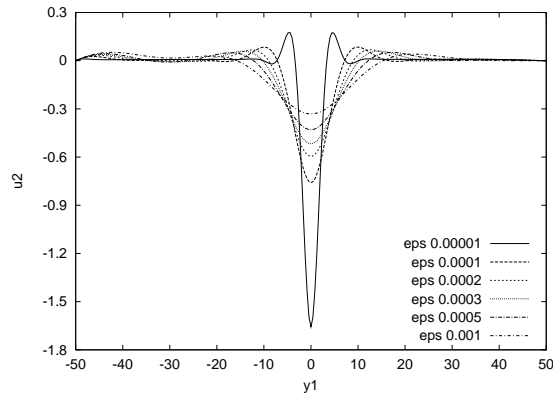
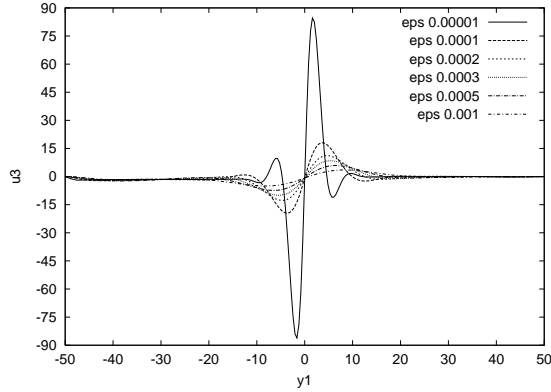
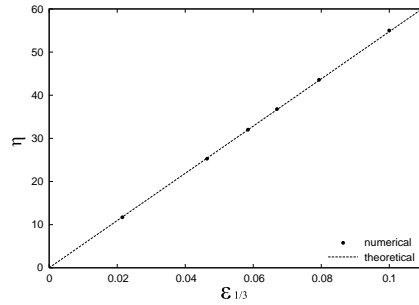


Figure 3.5: Displacement u_2^ε at $y^2 = 25$ for various ε

Figure 3.6: Displacement u_3^ε at $y^2 = 25$ for various ε Figure 3.7: Layer thickness η vs. $\varepsilon^{1/3}$

These three figures show that the displacements converge to the predicted distributions: u_1^ε to a Heaviside jump in $y^1 = 0$, u_2^ε to a δ and u_3^ε to a δ' (see Fig. A.1 in appendix A). A way to confirm the nature of these singularities is to study how the amplitudes vary with ε .

First, let us measure the corresponding internal layer thickness on the displacement u_3^ε . We take the thickness η as being the distance between the two extrema visible on Fig. 3.6. It is known (see for instance [14, 18]) that the thickness vary like $\varepsilon^{1/3}$ when an internal layer is along a characteristic line (here $y^1 = 0$). Fig. 3.7 shows a comparison between the numerical results and the theoretical ones which are in very good concordance.

Now, let us analyse the variation of the amplitude of u_2^ε and u_3^ε for the different values of ε . To this end, we shall consider the maximum of these two displacements. We recall that, according to the analysis developed in section 2, u_2^ε et u_3^ε tends respectively to be a Dirac singularity and its derivative. In appendix A, we recall that δ can be seen as the limit of a distribution whose support width is

η and amplitude is $1/\eta$ when η tends toward zero. If we take η as the thickness of the internal layer, the amplitude of u_2^ε should vary like $1/\eta$ i. e. $\varepsilon^{-1/3}$. With the same reasoning on δ' , we conclude that u_2^ε should vary like $\varepsilon^{-2/3}$. Figs 3.8 and 3.9 are in good agreement with that.

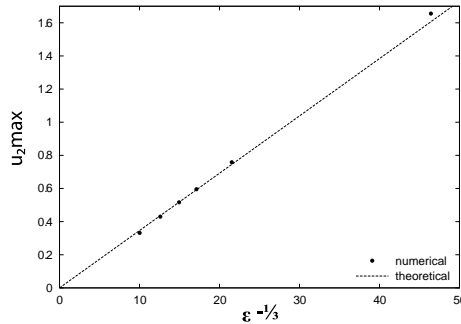


Figure 3.8: Value of u_{2max}^ε vs. $\varepsilon^{-1/3}$

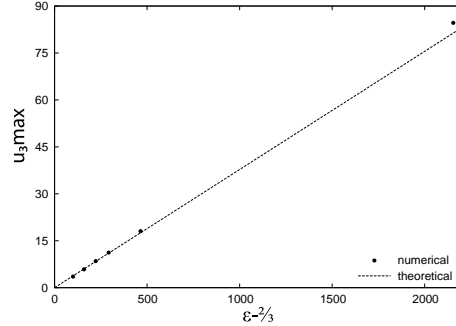


Figure 3.9: Value of u_{3max}^ε vs. $\varepsilon^{-2/3}$

On the other hand, all along the clamped boundary, we have a boundary layer. The most important one (in amplitude) is located along the edge AJ because AJ is also a boundary of the loading domain. As AJ is a characteristic line, the layer thickness should also be proportional to $\varepsilon^{1/3}$. Fig. 3.10 shows the normal displacement u_3^ε in this layer for various thicknesses.

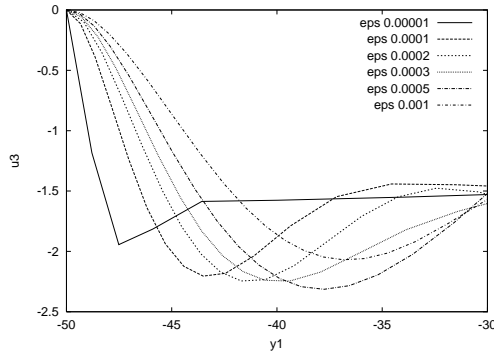


Figure 3.10: Displacement u_3^ε at $y^2 = 0$ for various ε

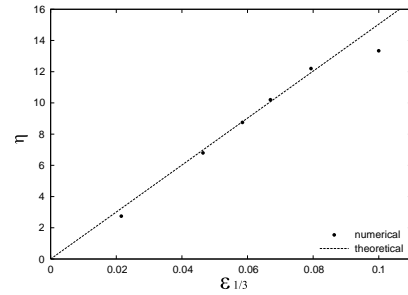


Figure 3.11: Boundary layer thickness η vs. $\varepsilon^{1/3}$

We can see on Fig. 3.10 that the description of the boundary layer is not so good for $\varepsilon = 10^{-5}$. In fact most elements concentrate in the internal layer where singularities are more important (in amplitude but not in order) and there are few elements outside. Without taking into account the value obtained for $\varepsilon = 10^{-5}$, we see that the layer thickness varies like $\varepsilon^{1/3}$ (see Fig. 3.11).

3.3 Results for the loading B

3.3.1 Mesh adaptation and displacements

We now consider loading B . The meshes obtained at various iterations are represented on Fig. 3.12. The evolution of the mesh is different from that of the case A because there is propagation of singularities. We can see that the mesh is refined along the loading domain boundary AOJ , but also along the characteristic lines tangent to the point O where the loading is locally singular in y^1 (see (2.27)) but also in y^2 (with the same orders as the singularity near $y^1 = 0$).

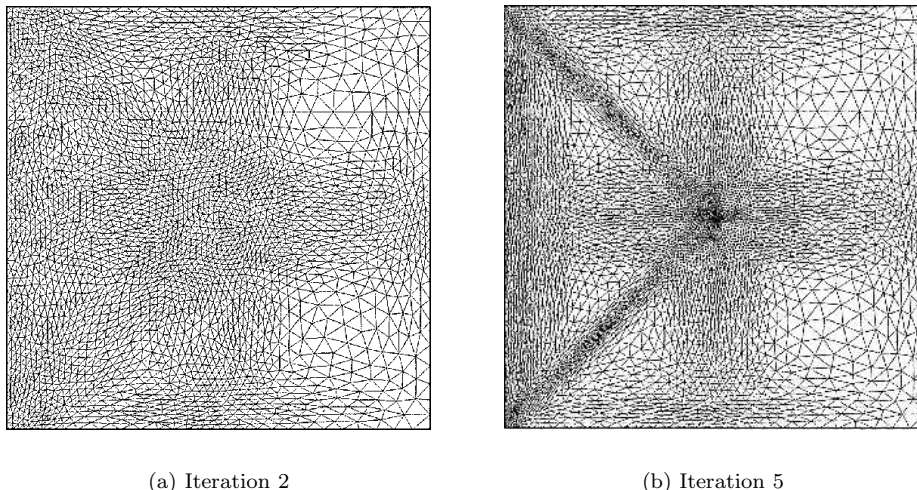


Figure 3.12: Evolution of the mesh during the adaptation process

Let us now consider the singularities of the displacements along the line $y^2 = 0$. In this case the order of the singularities of u_1 and u_2 are exchanged compared to the results presented in Tab. 2.1 (where the considered singularity was along the line $y^1 = 0$). The results concerning the two most singular displacements along the line $y^2 = 0$, *i. e.* u_1^ε and u_3^ε , are presented on figures 3.13 and 3.14 at $y^1 = 25$ *i. e.* on CH of Fig. 2.2.

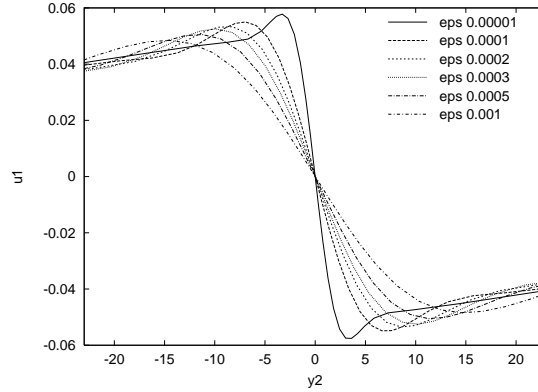


Figure 3.13: Displacement u_1^ε for $y^2 \in [-25, 25]$ and for various thicknesses

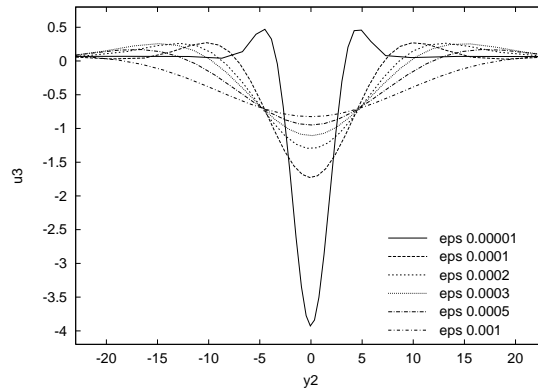


Figure 3.14: Displacement u_3^ε at $y^1 = 25$ for $y^2 \in [-25, 25]$ and for various thicknesses

In particular, we can notice that the singularities propagate along the characteristic line $y^2 = 0$ (as it is provoked by a singularity of the data at the origin). The displacement u_1^ε tends to be a Heaviside whereas u_3^ε tends to be a Dirac. The displacement u_2^ε is not presented here.

3.3.2 Comparison with structured meshes

Let us exhibit some numerical computations using uniform structured meshes. Fig. 3.15 displays the normal displacement for various meshes and for $\varepsilon = 10^{-5}$. We observe the efficiency of the adaptive process: adapted meshes of 34171 degrees of freedom (iteration 3) and 48437 DOF (iteration 7) give more accurate results than a structured uniform mesh with 71525 DOF (called S4). This last mesh is made of equal squares, each being divided in two triangles.

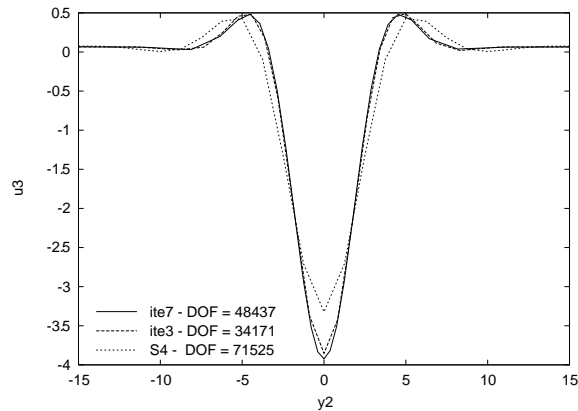


Figure 3.15: Displacement u_3^ε on the line $y^1 = 25$ for several meshes and for $\varepsilon = 10^{-5}$

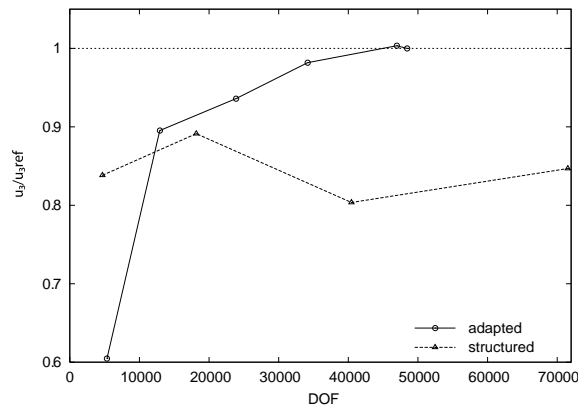


Figure 3.16: Comparison between the convergence of adapted and structured meshes - Normalized value of the normal displacement u_3^ε at the point $(y^1, y^2) = (25, 0)$ vs. number of DOF for $\varepsilon = 10^{-5}$

Fig. 3.16 shows the convergence of the results for $\varepsilon = 10^{-5}$ versus the number of DOF . The reference result u_{3ref} is that of the last iteration of the adaptive process though it may not be the exact result. We can see that the computations using adapted meshes converge much faster than those using structured meshes. The difference is not as important for thicker shells. This is due to the fact that the layers become very thin as ε tend to zero (like $\varepsilon^{1/2}$ or $\varepsilon^{1/3}$) and the elements need to be very thin and very elongated in the layers to get accurate results with a reasonable number of elements.

3.4 Results for the loading C

The meshes obtained at various iterations are plotted on Figs. 3.17(a) and 3.17(b). We can see that the mesh is refined along the loading domain boundary AOJ but also along the characteristic line $y^1 = 0$ tangent to the point O where the loading is locally singular in y^1 (see Fig. 2.2) but not in y^2 . A main difference is that this loading is not singular for $y^2 = 0$ and consequently, no propagation (or refinement) is seen along $y^2 = 0$.

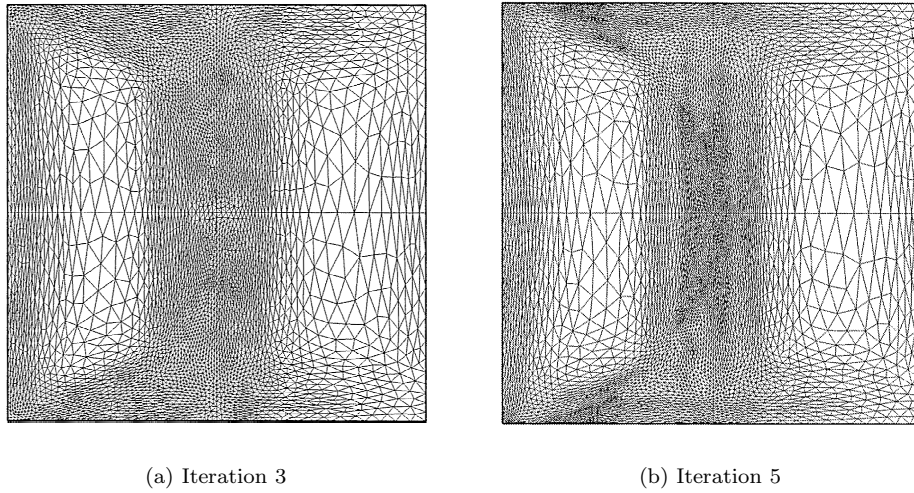


Figure 3.17: Evolution of the mesh during the adaptation process

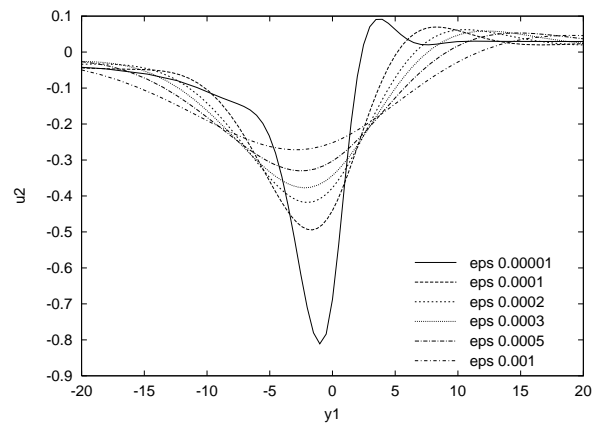


Figure 3.18: Displacement u_2^ε on the line $y^2 = 0$

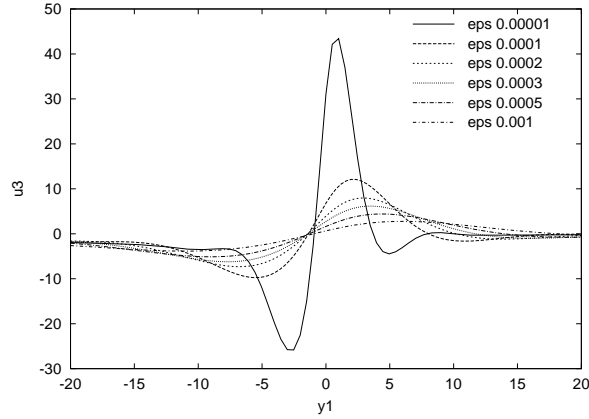


Figure 3.19: Displacement u_3^ε on the line $y^2 = 0$

The shapes of these two displacements do not enable us to determine accurately the type of singularity. We do not have one distinct oscillation as on figure 3.5 or two distinct oscillations as on figure 3.6. On figure 3.19, we can see one main oscillation, one intermediate and a last smaller. According to Fig. A.1, these singularities do not correspond to a δ or a δ' -like singularity. According to the results of table 2.1, the singularity of the displacement u_3^ε is between δ and δ' and that of the displacement u_2^ε between and Heaviside singularity H and a Dirac δ . That could be verified by studying respectively the variations of $|u_2^\varepsilon|_{max}$ and $|u_3^\varepsilon|_{max}$ when ε tends to zero.

4 Some examples including pseudo-reflections

Singularities propagating in hyperbolic shells enjoy non-classical properties of refraction (incidentally called pseudo-reflections) when arriving at a boundary. The main reason for a non-classical behaviour is that the boundary conditions are very different from those of classical Cauchy's problems of wave propagation, which lead to "classical reflection". These problems are far from completely solved, but some results are known from [15], from which the two following rules are taken (see Proposition 8.1 of [15]):

- *Rule 1*: when f^3 has a singularity of order ψ along a characteristic, u_3 bears a singularity of order ψ'' along that characteristic. When arriving at a simply supported (or clamped) boundary, the other characteristic issued from that point bears a singularity of order ψ' . This pseudo-reflection phenomenon does not occur when the boundary is free (in that case there is no reflection at all).

- *Rule 2*: when f^3 has a singularity of order ψ along a non-characteristic curve, u_3 bears also a singularity of order ψ along it. It has a non-propagating character, but it may arrive at a non-characteristic boundary provided that the support of the given singular loading arrives at it. In that case, the two characteristics issued from that point bear propagating singularities of order ψ or ψ' when the boundary is simply supported/clamped or free, respectively.

These rules are sufficient for understanding the examples in this section.

Let us consider the hyperbolic paraboloid defined by the same mapping (see (2.8)) with $c = 1$ but on the triangular domain of figures 4.1 and 4.2. This way, a part of the boundary (*i. e.* BC) is not along a characteristic line, which allows pseudo-reflection phenomena. Numerical computations are done with thickness 10^{-4} (and consequently relative thickness 2.5×10^{-5}).

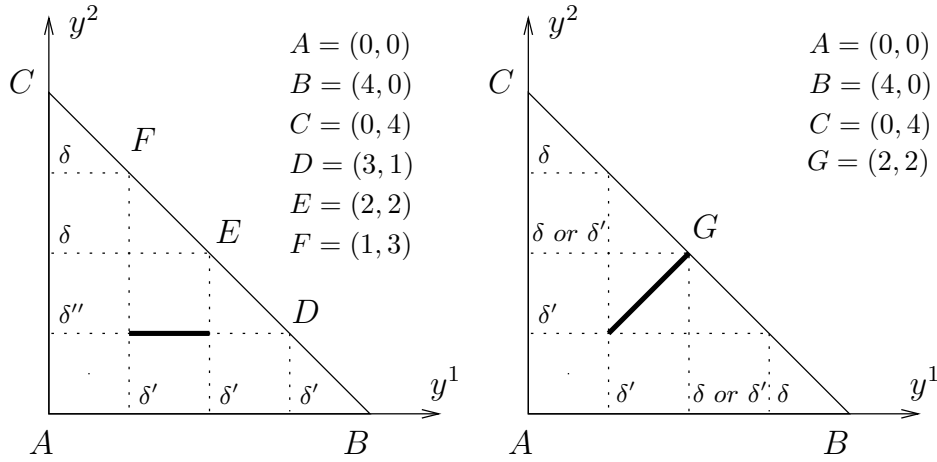


Figure 4.1: First problem

Figure 4.2: Second problem

4.1 Reflection of a characteristic layer

The first considered problem is similar to that of [13] but the computations are now performed with the adaptive mesh procedure. The shell is clamped along the part BC of the boundary and is consequently inhibited. A δ normal force with unit weight is applied on the segment $y^2 = 1$ with $1 \leq y^1 \leq 2$, specifically $f^3 = [H(y^1 - 1) - H(y^1 - 2)]\delta(y^2 - 1)$. As we saw in section 2.2, there is propagation of singularities for u_3 (see Fig. 4.1): δ' -like singularities propagate along the lines $y^1 = 1$ and $y^1 = 2$ whereas a δ'' -like singularity propagate along the line $y^2 = 1$.

Moreover, we have pseudo-reflection of the propagated singularity in δ'' as the boundary BC is not along a characteristic line (*Rule 1*). In the case considered here (reflection of a singularity along a characteristic line), the reflected singularity of u_3 at D is in δ' ; it is one order lower than that of the initial one. We also have reflections of the two other propagated singularities in δ' (along $y^1 = 1$ and $y^2 = 1$) in E and F , which give δ -like singularities along the lines $y^2 = 2$ and $y^2 = 3$. Note that there would be no reflection if the shell was free along BC .

We handled this problem numerically, using the adaptive and anisotropic remeshing procedure. The last mesh and results for u_3 are presented on Figs. 4.3 to 4.5.

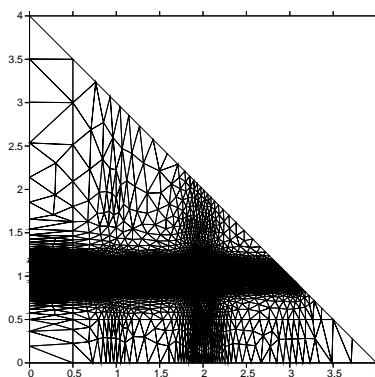


Figure 4.3: Mesh at the 5th iteration

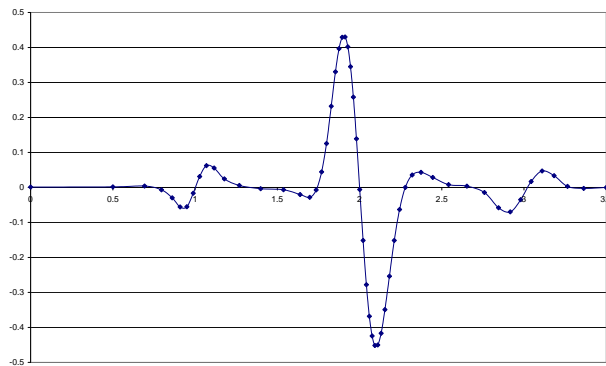


Figure 4.4: Displacement u_3 along the line $y^2 = 0.5$

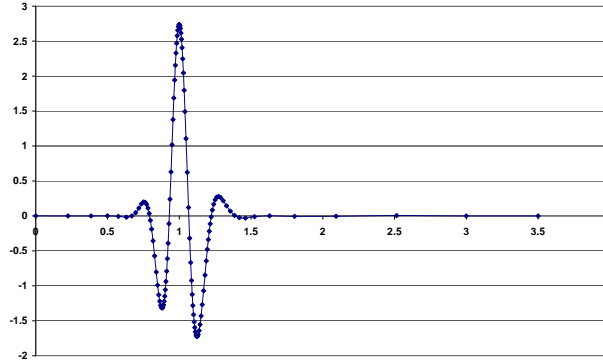


Figure 4.5: Displacement u_3 along the line $y^1 = 0.5$

We clearly observe that the mesh is mainly refined along the characteristic line $y^2 = 1$, corresponding to the discontinuity of the loading, and leading to a propagated δ'' -like singularity as seen previously (it is the higher order singularity).

Moreover, the mesh is also refined along the characteristic lines $y^1 = 1$ and $y^1 = 2$. As quoted above, the singularities also propagate along these characteristic lines, but are of a lower order (only in δ') than the previous one. So that the mesh is less refined than in the vicinity of the characteristic $y^2 = 1$. The mesh is also slightly refined along the characteristic line $y^1 = 3$, corresponding to the pseudo-reflection of the singularity of u_3 at the fixed edge. Finally, there is no refinement along the lines $y^2 = 2$ and $y^2 = 3$ where the existing singularities are negligible ("only" in δ).

Fig 4.4 displays u_3 along the line $y_2 = 0.5$ exhibiting three δ' -like singularities ("double oscillations"). The two first ones, at $y^1 = 1$ and $y^1 = 2$ are those propagated from the extremities of the applied loading, whereas the third one, at $y^1 = 3$ is the pseudo-reflected from D (see Fig. 4.2). It has to be noted that this last one is weaker than the original singularity, in order (δ' against δ'') but also in amplitude (0.05 against 2.5). Figure 4.5 displays u_3 along the line $y_1 = 0.5$, exhibiting the singularity of the highest order (δ'' -like or "triple oscillation").

4.2 Reflection of a non-characteristic layer

Let us now consider the second situation (Fig. 4.2). The shell is now subjected to a δ normal loading with unit weight along the line $y^1 = y^2$ for $1 \leq y^1 \leq 2$. This loading can be written $f^3 = \delta(y^1 - y^2)H(y^1 - 1)H(y^2 - 1)$. The loading is singular along a non-characteristic line which has an intersection with the boundary BC (which is a boundary along a non-characteristic line). According to *Rule 2*, the singularity of the displacement u_3 is of the same order as that of the loading f^3 (but there is no propagation). Consequently, u_3 has a δ -like singularity along the line $y^1 = y^2$ (for $1 \leq y^1 \leq 2$). Moreover, there are some

classical propagated singularities of u_3 along the lines $y^1 = 1$ and $y^2 = 2$. On the other hand, according to *Rule 2*, some reflected singularities also appear on the two characteristic lines issued from the point $G = (2, 2)$ which is the intersection between the loading domain and the boundary BC . The order of the singularity of u_3 in these two reflected layers depends on the boundary condition along the boundary BC . When BC is clamped (respectively free), u_3 has a δ - like singularity (respectively a δ' - like singularity).

Let us observe the numerical results for two types of boundary conditions:

(a) the shell is clamped along BC and free elsewhere

(b) the shell is free along BC and clamped elsewhere

With any of these two boundary conditions, the shell is inhibited.

4.2.1 Case a

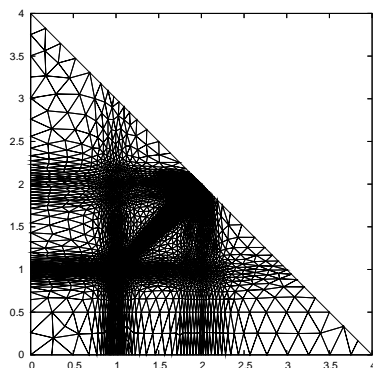


Figure 4.6: Refined mesh for the first problem

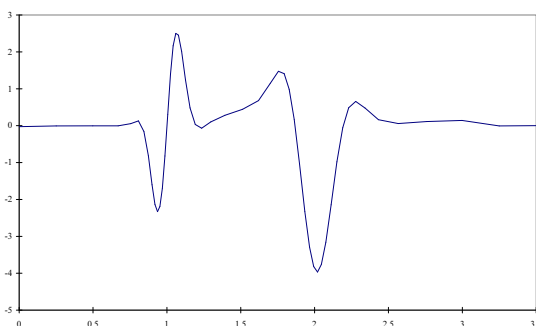


Figure 4.7: Displacement u_3 on the line $y^2 = 0.5$ in case a

According to *Rule 2*, the singularity of u_3 arriving at the boundary BC reflects. As the shell is clamped along BC , the reflected singularity is of the same order as the initial one. Figure 4.6 clearly shows that the mesh is refined along five layers:

- three classical layers where the mesh is strongly refined, along the loading domain and the characteristic lines $y^1 = 1$ and $y^2 = 1$ issued from the discontinuity of the loading
- two reflected layers along the lines $y^1 = 2$ and $y^2 = 2$.

The other reflected singularities are negligible. Figs. 4.7 clearly shows that δ' - like singularity (two oscillations) along $y^1 = 1$ and the δ - like singularity (one main oscillation) along the line $y^1 = 2$.

4.2.2 Case b

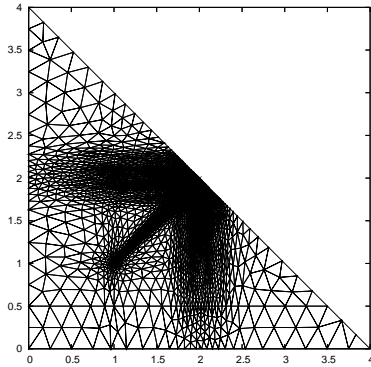


Figure 4.8: Refined mesh for the second problem

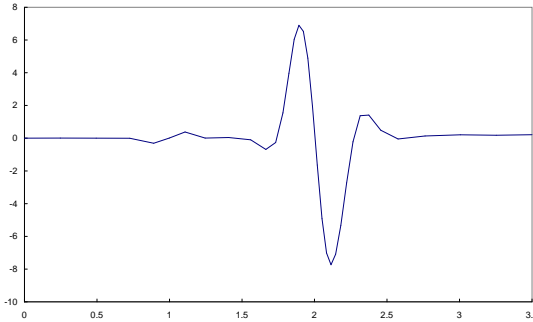


Figure 4.9: Displacement u_3 on the line $y^2 = 0.5$ in case b

In this case, as the shell is free along BC , the reflected singularities are one order more singular than the initial one (*Rule 2*). Figure 4.8 displays the mesh of the last iteration: it is here clearly refined along the reflected layers which are the most important ones (δ' -like). The classical propagated singularities (which are δ' -like too) are less important because of the boundary conditions. On Fig. 4.9, we see two δ' -like singularities: in $y^1 = 1$ there is a small singularity (in amplitude) whereas the reflected singularity in $y^1 = 2$ is much more important.

The previous examples show that despite the various types of layers (propagated or reflected), the automatic and adaptive numerical procedure allows to get accurate results for the normal displacement by refining automatically the mesh where it needs to be. Doing a manual refinement needs *a priori* knowledge of all the existing singularities, their order and amplitude everywhere on the shell. It would have been much longer in the two considered examples, and would be nearly impossible in general for complex shell geometries and loadings.

5 Use of anisotropic meshes for non-inhibited shell problems

In this section, we will see how the numerical procedure can reduce membrane locking when the shell is not inhibited. In this case, the middle surface naturally deforms with inextensional displacements and the Koiter model tends to a pure bending problem when ε tends to zero. For such problems, it is known that membrane locking occurs and leads to an important underestimate of the displacement when the relative thickness ε decreases. Locking is usually defined

[1] as non-uniformity with respect ε of the convergence of the F.E. process. In particular, this implies non-commutativity of the limits $\varepsilon \searrow 0$ and $h \searrow 0$ (where V_h is the F. E. space). As a matter of fact, when the shell is not inhibited, the solutions of the limit $\varepsilon \searrow 0$ are in G . Correspondingly, the limit when $\varepsilon \searrow 0$ of the solutions of the numerical approximation in V_h are in $V_h \cap G$. In most cases, $V_h \cap G$ reduces to the zero element, rendering commutativity impossible and locking arises.

Examples of membrane locking can be seen in [9] for hyperbolic shells or in [17] for parabolic ones.

Let us consider the following problem.

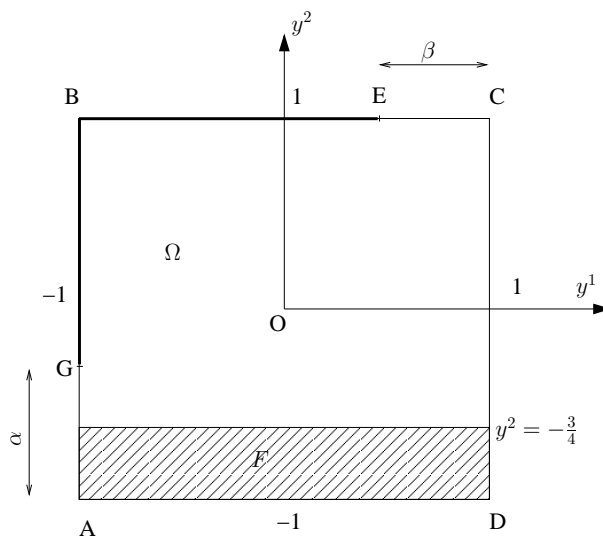


Figure 5.1: Domain in \mathbb{R}^2

We still consider the same hyperbolic paraboloid defined by the mapping (2.8) with $c = 1$. The reference domain of the local variables (y^1, y^2) is that of Fig 5.1. The shell is clamped along the edges BG and BE , the distances EC and GA being respectively equal to β and α which are taken as parameters. A constant normal loading is applied on the hatched area. When β and α vary, the non-inhibited area will be more or less important.

5.1 First case: $\alpha = 0$ and $\beta = 0.25$

In this case, the shell is only non-inhibited in the rectangle $[0.75, 1] \times [-1, 1]$. In fact, referring to the considerations on rotations given in the introduction, we could say that this zone is "partially-inhibited" because of the whole family of

characteristics $y^2 = \text{const}$ is clamped at $y^1 = -1$ and rotations around them are prevented. Only rotations around $y^1 = \text{const}$ for $0.75 < y^1 < 1$ are allowed.

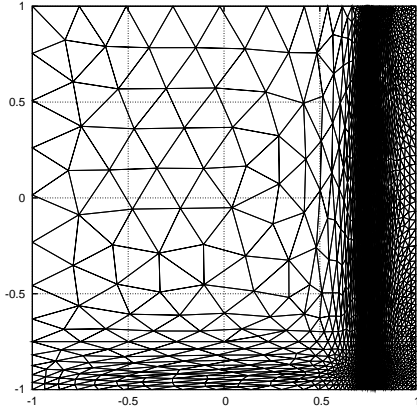


Figure 5.2: Mesh at the 5th iteration

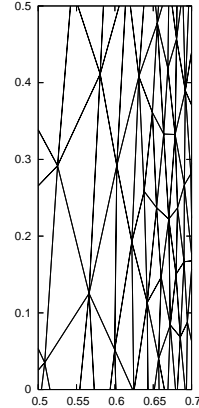


Figure 5.3: Zoom of the mesh

On Fig. 5.2, we can see that the mesh is mainly refined along the line $y^1 = 0.75$ which is the border of the non-inhibited zone. In this zone the mesh is strongly anisotropic (anisotropy factor of about 10, see Fig. 5.3) in order to describe the bending which occurs around the direction $y^1 = \text{const}$. Moreover, the mesh is also refined anisotropically along the lines $y^2 = -0.75$ and $y^2 = -1$ corresponding to an internal and a boundary layer due to the loading in the inhibited domain.

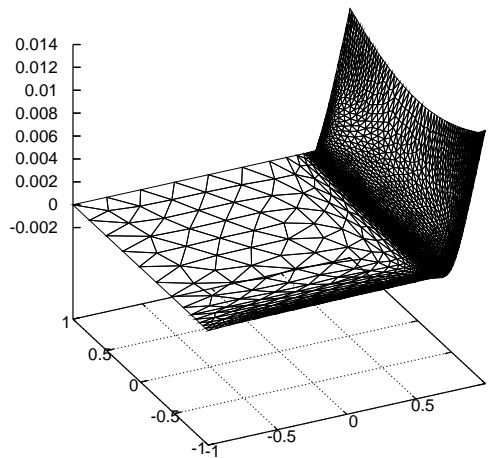


Figure 5.4: Displacement u_3

On Fig. 5.4, we can see that the displacements are much more important

in the non-inhibited region, and also significant in the two layers. This put in a prominent position the capacity of the remeshing procedure to describe automatically phenomena qualitatively and quantitatively very different.

5.2 Second case: $\alpha = 0.25$ and $\beta = 0.25$

The shell is now non-inhibited on a more important area composed of three "subareas". In the rectangle $[0.75, 1] \times [-0.75, 1]$, only the bending in the direction $y^1 = \text{const}$ is allowed, whereas it is only allowed in the direction $y^2 = \text{const}$ in the rectangle $[-1, 0.75] \times [-1, -0.75]$. Finally, the rectangle $[0.75, 1] \times [-1, -0.75]$ admits bending in the two directions and is "completely non-inhibited".

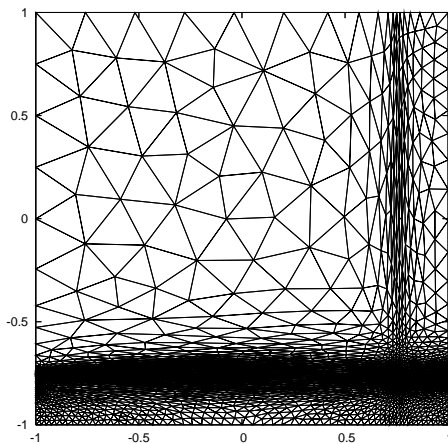


Figure 5.5: Mesh at the 5th iteration

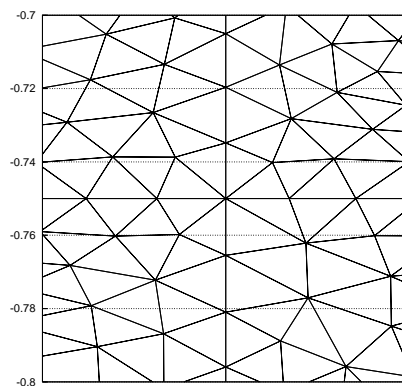
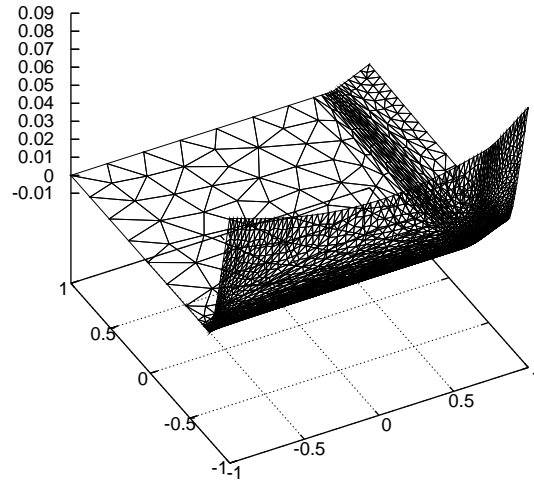


Figure 5.6: Zoom of the mesh around the point $(0.75, -0.75)$

The automatic refinement is now performed mainly along the lines $y^1 = 0.75$ and $y^2 = -0.75$, where the anisotropy factor of the elements (in the directions y^1 and y^2) reaches 20. In the totally "non-inhibited domain", as the bending is allowed in both directions, the mesh is nearly isotropic (see Fig. 5.6). The little anisotropy (anisotropy factor about 1.5) is caused by the non-symmetrical loading.

Figure 5.7: Displacement u_3

Displacement u_3 is plotted on Fig. 5.7: it is important in the tree non-inhibited areas but reaches its maximum in the totally "non-inhibited domain", which is moreover subjected to the normal loading.

It is interesting to observe the repartition of membrane and bending energies as this problem contains inhibited and non-inhibited regions. The percentage of bending energy surface density with respect to the total energy surface density is displayed on Fig. 5.8.

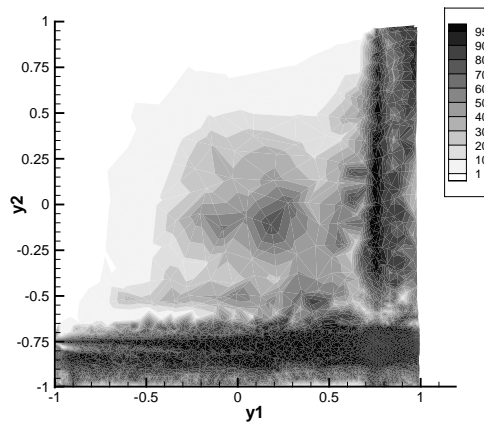


Figure 5.8: Percentage of bending energy surface density

In the inhibited region, membrane energy is dominating, which corresponds to the membrane limit behaviour. Bending energy surface density is concentrated

along the characteristics $y^2 = -0.75$ and $y^1 = 0.75$ which behave like "hinges" (about 95% of the total energy surface density). It is still important in the rest of the partially inhibited domain (about 70 – 80%). Moreover, bending energy is dominating in the "totally inhibited region" (80 – 95%).

6 Conclusion

In the first part of this paper we established some theoretical results on the limit behavior of hyperbolic inhibited shells. When the loading is singular, we deduced the most singular term of the resulting displacements. In particular, we proved that the normal displacement u_3 is two orders more singular than the normal loading f^3 when f^3 is singular along a characteristic line, and only as singular as f_3 when f_3 is singular on a non characteristic line. For thin shells, the solutions exhibit internal layers where functions vary drastically in the normal direction. Accurate numerical computations are then obtained via an adaptive and anisotropic mesh procedure which enables us to refine automatically the mesh inside the layers, mainly in the direction normal to the layer. The numerical results obtained for very thin hyperbolic shells are in good agreement with the theory: we recover the theoretical results for displacements amplitudes and for layers thicknesses. Moreover, we showed the advantage of such an automatic anisotropic remeshing compared to uniform meshes which require much more elements to obtain similar results especially when the shell is thin.

Finally, we show the pertinence of the automatic character of the adaptive re - meshing, specially in entangled situations of the real world, where the theoretical description of the asymptotic behavior is practically impossible (think to cases involving repeated pseudo reflections, or cases where both bending and membrane dominated regions are present in the shell).

A Appendix: Some recalls about distributions

Let us specify the terminology used in this paper for describing singularities. Let $S_0(x)$ be a basic singularity. Then, we have the corresponding chain:

$$(A.1) \quad \dots S_{-2}(x), S_{-1}(x), S_0(x), S_1(x), S_2(x), S_3(x), \dots$$

with $S_{k+1} = \frac{d}{dx} S_k$. This chain of singularities must be understood in the sense of functions (or distributions) defined up to an additive function (or distribution) which is smooth in the neighborhood of x . Thus, we say that $S_2(x)$ is 2 orders more singular than $S_0(x)$ and $S_{-2}(x)$ is 2 orders less singular than $S_0(x)$. An example is:

$$(A.2) \quad \dots x H(x), H(x), \delta(x), \delta'(x), \dots$$

$H(\cdot)$ being the Heaviside jump function and $\delta(\cdot)$ the Dirac function, but there are many other ones. In order to interpret numerical results, we recall that the Dirac distribution δ corresponds to the limit of a function having a support length equal to η and an amplitude equal to $1/\eta$ when η tends toward zero. The

distribution δ' being the derivative of δ , it has the same support of length η , an amplitude $1/\eta^2$ and one more oscillation. That characterizes the family of singularities $\delta, \delta', \delta'' \dots$ (see Fig. A.1)

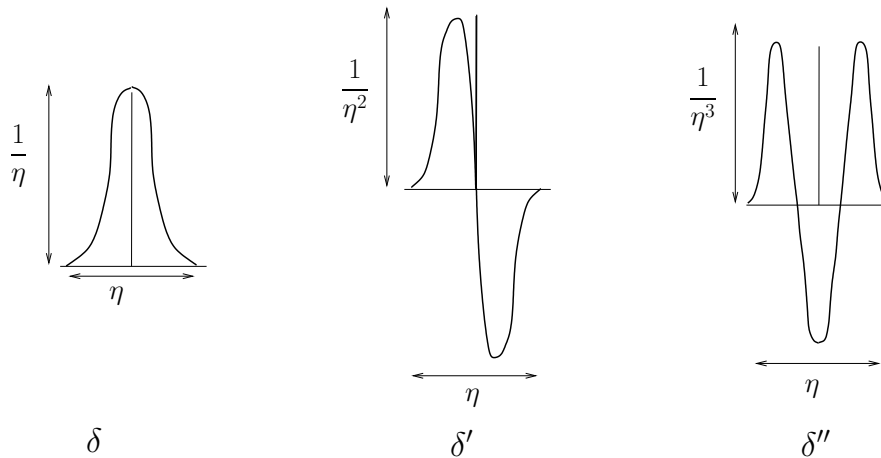


Figure A.1: Heuristic patterns of δ singularity family

Acknowledgment. The authors are indebted to the referees for remarks and comments which allowed improvements and helped to eliminate some mistakes in the text.

REFERENCES

1. I. Babuska & M. Suri, *On locking and robustness in the finite element method*, J. Numer. Anal, 29 (1992) pp. 1261–1293.
2. F. Béchet, E. Sanchez-Palencia & O. Millet, *Computing singular perturbations for elliptic clamped shells*, Computational Mechanics, 42 (2008) pp. 287–304.
3. F. Béchet, E. Sanchez-Palencia, O. Millet, *Computing singular perturbations generating complexification phenomena*, to appear in Computational Mechanics, 2008.
4. M. Bernadou, *Méthodes d'éléments Finis pour les Problèmes de Coques Minces*, Masson, 1994.
5. H. Borouchaki, P.L. George, F. Hecht, P. Laug, E. Saltel, *Delaunay mesh generation governed by metric specifications. Part I. Algorithms*, Finite Elements in Analysis and Design, 25 (1997) pp. 61–83.
6. H. Borouchaki, F. Hecht, P.J. Frey, *Mesh gradation control*, Int. J. Numer. Meth. Engng., 43 (1998), pp. 1143–1165.
7. M. J. Castro-Diaz, F. Hecht, B. Mohammadi and O. Pironneua, *anisotropic unstructured mesh adaptation for flow simulations*, IJNMF, 25 (1997), pp. 475–491.
8. D. Caillerie, A. Raoult, E. Sanchez-Palencia, *On internal and boundary layers with unbounded energy in thin shell theory. Hyperbolic characteristic and non-characteristic cases.*, Asymptotic Analysis, 46 (2006), pp. 189–220.

9. D. Choï, *Computations on non-inhibited hyperbolic elastic shells. Bench-mark for the membrane locking*, Journal Mathematical Methods Applied Sciences, 22 (1999), pp. 1293–1321.
10. C.A. De Souza, *Techniques de maillage adaptatif pour le calcul des solutions de coques minces*, PhD Thesis, University Paris VI, 2003.
11. C.A. De Souza, D. Leguillon, É. Sanchez-Palencia, *Adaptative mesh computation for a shell-like problem with singular layers.*, International Journal for Multiscale Computational Engineering, 1 (2003), pp. 401–417.
12. P.L. George: *Maillage et adaptation*, Hermes, 2001.
13. P. Karamian, J. Sanchez-Hubert, É. Sanchez Palencia, *Non-Smoothness in the asymptotics of thin shells and propagation of singularities. Hyperbolic case*, Int J.Appl. Math. Comp. Sci., 12 (2002), pp. 81–90.
14. P. Karamian, J. Sanchez-Hubert, É. Sanchez Palencia, *Propagation of singularities and structure of layers in shells. Hyperbolic case*, Computers and Structures, 80 (2002), pp. 747–768.
15. P. Karamian, J. Sanchez-Hubert, É. Sanchez Palencia, *Pseudo-reflection phenomena for singularities in thin elastic shells*, Math. Meth. Appl. Sci., 26 (2003), pp. 1451–1485.
16. W.T. Koiter, *The theory of thin elastic shells*, North-Holland, Amsterdam, 1959.
17. J. Pitkäranta, *The problem of membrane locking in finite elements analysis of cylindrical shells*, Numerische Mathematik, 61 (1992), pp. 523–542.
18. J. Pitkaranta, A.-M. Matache, C. Schwab, *Fourier mode analysis of layers in shallow shell deformations*, Comp. Meth. Appl. Mech. Engrg. 190 (2001), pp. 2943–2975.
19. J. Sanchez-Hubert, É. Sanchez-Palencia, *Coques élastiques minces - Propriétés asymptotiques*, Masson, Paris, 1997.
20. J. Sanchez-Hubert, É. Sanchez-Palencia, *Singular perturbations with non-smooth limit and finite element approximation of layers for model problems of shells*, Partial Differential Equations in Multistructures, Dekker, New York, 2001, pp. 207–226.
21. J. Sanchez-Hubert, É. Sanchez-Palencia, *Anisotropic finite element estimates and local locking for shells: parabolic case*, C. R. Acad. Sci., Sér. IIB, 329 (2001), pp. 153–159.